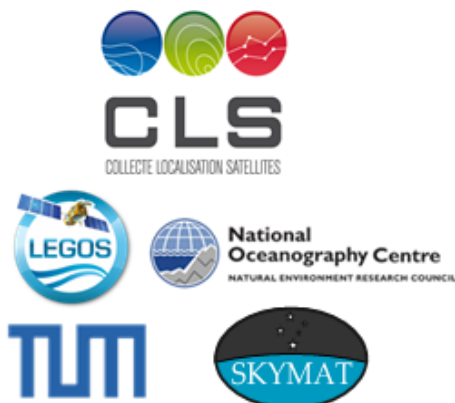




ESA/Contract No. 4000126561/19/I-NB

Consortium Members



ESA Sea Level CCI+

CCN2 TUM D1.1

Reference:

Nomenclature: SLCCI+_CCN2_D1.1_043_TUM_v2

Issue: 2.0

Date: Mar. 16, 22





Chronology Issues:			
Issue:	Date:	Reason for change:	Author
1.0	30/07/21	Initial Version	J. Oelsmann, M. Passaro
2.0	16/03/22	Revised Version	J. Oelsmann

People involved in this issue:		
Written by:	J. Oelsmann	
Checked by:	JF Legeais (CLS)	
Approved by:	JF Legeais (CLS)	

Acceptance of this deliverable document:			
Accepted by ESA:	J. Benveniste (ESA)		

Distribution:		
Company	Names	Contact Details
ESA	J. Benveniste A. Ambrozio, M. Restano	Jerome.Benveniste@esa.int ; Americo.Ambrozio@esa.int ; Marco.Restano@esa.int
CLS	J.-F. Legeais ; P. Prandi ; S. Labroue ; A. Guerou	jlegeais@groupcls.com ; pprandi@groupcls.com ; slabroue@groupcls.com ; aguerou@groupcls.com ;
LEGOS	A. Cazenave ; B. Meyssignac ; F. Birol; F. Nino; F. Leger;	anny.cazenave@legos.obs-mip.fr ; Benoit.Meyssignac@legos.obs-mip.fr ; florence.biol@legos.obs-mip.fr ; fernando.nino@legos.obs-mip.fr ; fabien.leger@legos.obs-mip.fr ;
NOC	F. Calafat	Francisco.calafat@noc.ac.uk ;
SkyMAT Ltd	A. Shaw	agps@skymat.co.uk ;
DGFI-TUM	M. Passaro J. Oelsmann	marcello.passaro@tum.de julius.oelsmann@tum.de



List of tables and figures

Figures

- Figure 1: *Along-track correlations based on monthly PSMSL and XTRACK-ALES data for selected stations. Correlations are computed with respect to the nearest TG within a radius of 300 km (in the zone of influence). Note, that some of the correlations of two neighbouring TG stations might overlap in this figure. The blue shading indicates the bathymetry. 9*
- Figure 2: *Along-track correlations based on monthly PSMSL and XTRACK-ALES data. The 20% best correlated points are highlighted with blue borders..... 10*
- Figure 3: *Shown are SLA time series of altimetry and TG data as well as the differences of SLAs for selected stations and different coupling criteria: rms, cor and PoHC. Note, that the closest point is not shown, due to the larger discrepancies of the TG and altimetry data for this selection. 13*
- Figure 4: *Correlations of monthly SAT and TG (PSMSL) observations (both detrended + deseasoned). The SAT SLA time series are computed based on the different criteria: (a-c) 20% best correlations, rms or residual annual cycle, the closest point (d), as well as the point of highest correlation (e). The boxplot (f) shows the distribution of correlations (the median and lower and upper quartile ranges). 14*
- Figure 5: *Trend uncertainties (mm/year) of SAT-TG VLM. VLM is computed based on the different criteria: (a-c) 20% best correlations, rms or residual annual cycle, the closest point (d), as well as the point of highest correlation (e). The boxplot (f) shows the distribution of trend uncertainties (the median and lower and upper quartile ranges). In (f) we additionally show the results (orange), in case a correlation threshold of 0.6 is applied (based on the correlations of the time series based on the ZOI + cor criterium with monthly TG data). 15*
- Figure 6: *Driving noise (mm) of SAT-TG VLM. VLM is computed based on the different criteria: (a-c) 20% best correlations, rms or residual annual cycle, the closest point (d), as well as the point of highest correlation (e)..... 16*
- Figure 7: *Spectral index of SAT-TG VLM. VLM is computed based on the different criteria: (a-c) 20% best correlations, rms or residual annual cycle, the closest point (d), as well as the point of highest correlation (e)..... 17*
- Figure 8: *Trends (mm/year) of SAT-TG VLM. VLM is computed based on the different criteria: (a-c) 20% best correlations, rms or residual annual cycle, the closest point (d), as well as the point of highest correlation (e). The boxplot (f) shows the distribution of trends (the median and lower and upper quartile ranges). In (f) we additionally show the results (orange), in case a correlation threshold of 0.6 is applied (based on the correlations of the time series based on the ZOI + cor criterium with monthly TG data). 18*
- Figure 9: *Boxplots of differences of SAT-TG VLM (XTRACK-ALES - PSMSL) and GNSS VLM. The data are grouped according to the distance between TG and GPS station, as well as a correlation threshold of 0.6. The correlation threshold is based on the XTRACK-ALES and TG data (ZOI-cor criterium). 19*
- Figure 10: *VLM (a-c) and uncertainties (d-e) for different SAT-TG combinations (XTRACK-ALES, OpenADB-ALES, CMEMS). For all datasets the ZOI-cor criterium to construct the SAT-TG time series was used. 22*
- Figure 11: *Histograms of trend differences (SAT-TG minus GNSS VLM) of the different altimetry dataset for different maximum allowed distances between TG and GNSS station: a) 1 km b) 50 km 22*
- Figure 12: *Problematic SATTG VLM time series, which are edited (a,b) or rejected (c,d) from the dataset. In a) the time series is truncated to the years 2005-2019, in b) the data after*



2016 is rejected. Dashed vertical lines indicate possible discontinuities after manual inspection. 25

Figure 13: Continuous VLM (a) and uncertainties (b) along the European coastline. In addition to the continuous interpolated estimate, we show the SATTG VLM and uncertainties (white edge-colours). 27

Figure 14: Continuous VLM (a) and uncertainties (b) on Oceania and South-East Asia. In addition to the continuous interpolated estimate, we show the SATTG VLM and uncertainties (white edge-colours). 28

Figure 15: Continuous VLM and uncertainties along the European a) and the Australian b) coastline. The green line shows the posterior mean estimate, the orange shading encapsulates the 2-sigma confidence intervals of the interpolated VLM. SATTG VLM and uncertainties are shown in purple. 29

Tables

Table 1: Summary of statistics of the combination of monthly XTRACK-ALES and PSMSL data for all regions and available TGs. We show the median of correlations, VLM trends and uncertainties, as well as the median driving noise and the spectral index. 10

Table 2: Comparison of SAT-TG VLM (XTRACK-PSMSL) and GNSS VLM. Shown are the RMS of trends and the median bias of differences for all data (as well as for a sub-selection with a correlation threshold of 0.6). The correlation threshold is based on the XTRACK-ALES and TG data (ZOI-cor criterium). 19

Table 3: Comparison of SAT-TG VLM (XTRACK-PSMSL) and GIA (+CMR) VLM. Shown are the RMS of trends and the median bias of differences for all data (as well as for a sub-selection with a correlation threshold of 0.6). The correlation threshold is based on the XTRACK and TG data (ZOI-cor criterium). 20

Table 4: Comparison of GNSS VLM with SAT-TG VLM which are based on the XTRACK-ALESS (ZOI-cor), CMEMS (ZOI-cor), OpenADB-ALES (ZOI-cor) altimeter datasets and PSMSL TGs. Shown are the RMS, the standard-deviations and the median bias of VLM differences for all data, as well as for a sub-selection with a correlation threshold of 0.6. The correlation threshold is based on the XTRACK-ALES and TG data (ZOI-cor criterium). 21

Table 5: Dataset description of the deliverable DGFI_VLM_XTRACK_ALES_PSMSL_<criterion>_<vlm_version>_<sla_version>, consisting of point-wise VLM information derived from SAT-TG. We provide five different netCDF files, which contain VLM information for all applied SAT selection criteria (<criterion>). <vlm_version> refers to the dataset version and <sla_version> refers to the XTRACK-ALES SLA version number. 23

Table 6: Dataset description of the deliverable DGFI_2D_VLM_MAPS_XTRACK_ALES_PSMSL_RMS_v1_v1.1_202006, consisting of interpolated VLM data derived from SAT-TG. 29

Applicable documents

AD 1 Sea level CCI project Management Plan
SLCCI+_PMP_003_ProjectManagementPlan

List of Contents

1. Introduction and task description 6



2. D1.1 + D1.2 Alt-TG VLM estimates	7
2.1. Data and Methods.....	7
2.1.1. Data.....	7
2.1.2. Methods and algorithm description	8
2.2. Validation results	9
2.2.1. Comparison of different data-selection approaches: XTRACK - PSMSL	9
2.2.1.1. XTRACK-ALES - PSMSL Comparison of the statistics: cor, rms, AC, closest, PoHC .10	
2.2.1.2. XTRACK-ALES - PSMSL Comparison of SAT-TG VLM and GNSS VLM	11
2.2.2. XTRACK-ALES - PSMSL Comparison with GIA models	20
2.2.3. Comparison with other altimetry datasets	21
2.2.3.1. Discussion of the altimetry trend biases	22
2.3. Dataset description.....	23
3. D3 - Alt-TG VLM: Regional Map	25
3.1. Method	25
3.1.1. Data preprocessing - outlier rejection	25
3.1.2. 2D interpolation - Transdimensional regression.....	26
3.2. Results	27
3.3. Dataset description.....	29
4. References.....	30



1. Introduction and task description

This report describes the algorithms employed and validation results of the tasks 1.1 + 1.2 and 1.3. The main goal of the investigations is the improvement of coastal vertical land motion (VLM) estimates derived from the differences of satellite altimetry and tide-gauge observations (see, e.g. Wöppelmann and Marcos, 2016). Understanding and estimating VLM is critical to quantify the rates of coastal relative sea level change. Most of global VLM observations stem from the Global Positioning System (GPS). Since more than two decades VLM from differences of absolute (satellite altimetry) and relative sea level (tide gauge) measurements (SAT-TG) have been exploited to improve and densify VLM along the coastlines (e.g., Cazenave et al., 1999). Linear VLM rates from GPS are more accurate (0.6 mm/year, Santamaria-Gomez et al., 2012) than those from SAT-TG (1.2-1.8 mm/year, Kleinherenbrink et al., 2018; Pfeffer and Allemand, 2016). Ideally, the uncertainties should be one order of magnitude less than contemporary rates of absolute sea level change, i.e., 1-3 mm/year (see, e.g., Wöppelmann and Marcos, 2016, hereinafter called WM16).

In order to enhance the accuracy and precision of SAT-TG VLM estimates, advanced coastal altimetry datasets as well as refined coupling approaches of SAT and TG observations have been applied. Developments and rapid improvements in the recent years by e.g. application of coastal-retracking and advanced geophysical corrections (e.g., Cipollini et al., 2017; Passaro et al., 2014; Fernandes et al., 2015) have improved sea level observation especially in the coastal zones. Dedicated coastal altimetry datasets might thus outperform previously applied products, which do not yet benefit from these implementations.

Next to issues concerning data quality also the spatial selection of altimeter data in the vicinity of the TG influenced the residual VLM time series quality. WM16 showed, that averaging SLA in a radius of 1° around the TG resulted in higher correlations than using the best correlated or the closest grid point to the TG. Kleinherenbrink et al., 2018, found a small influence of variations of absolute correlation thresholds on the trend estimates. Therefore, an advanced adaptation of the choice of altimetry SLA might improve representation of the signal captured by the TG and reduce the noise in the residual VLM time series.

Thus, this work shall contribute to further explore improvements by using dedicated coastal altimetry products (XTRACK-ALES) as well as different coupling schemes of SAT and TG observations. Furthermore, the results based on the 16 year long Jason altimetry data, will also be compared to longer multimission datasets (OpenADB-ALES) and gridded products (CMEMS, previously called AVISO in WM16, see data-section 2.1.1). The following figure summarizes the tasks to be fulfilled within this phase.

Task 1.1	Task 1.2	Task 1.3
<ul style="list-style-type: none"> • Computation of Zone of influence (ZOI) using 20% of the best data based on correlation (corr), root-mean-square error (rms), residual annual cycle • SAT-TG VLM based on closest point and point of highest correlation (PoHC) w.r.t. TGs from the Permanent Service for Mean Sea Level (PSMSL) • Identification of outliers using objective criteria (e.g., correlation) 	<ul style="list-style-type: none"> • Comparison of performances of VLM uncertainties + accuracy (obtained from the comparison with GNSS trends) w.r.t.: ➤ Different SAT selection criteria (ZOI, PoHC) ➤ Different outlier criteria, GNSS and TG distance ➤ Different altimetry datasets: Adaptive Leading Edge Subwaveform (ALES) Retracker, CMEMS 	<ul style="list-style-type: none"> • Production of SAT-TG VLM dataset for the provided regions • Computation of VLM uncertainties • Comparison with large scale Glacial Isostatic Adjustment (GIA) + Contemporary mass redistribution (CMR) estimates

We present the results of the tasks 1.1 + 1.2 in section 2. The analysis of the regional interpolated VLM map (task 1.3) can be found in section 3.



2. D1.1 + D1.2 Alt-TG VLM estimates

2.1. Data and Methods

2.1.1. Data

Sl_cci+ coastal sea level product

We use 20Hz along-track sea level anomalies (SLAs) from the XTRACK-ALES product (version v1.1_202006). SLA observations were obtained by the Jason 1,2 and 3 missions and cover the period from 15 January 2002 to 30 May 2018. The altimetry data is adjusted for the atmospheric effects (wet and dry troposphere, ionosphere, inverse barometer), geophysical phenomena (ocean tides, high frequency atmospheric effects on the ocean) and the sea-surface state (electromagnetic seasurface bias), see Birol et al., 2021 for a more detailed list. The product is available at https://doi.org/10.5270/esa-sl_cci-xtrack_ales_sla-200206_201805-v1.1-202005. The product User Guide (currently v1.3, available at: <https://climate.esa.int/en/projects/sea-level/key-documents/>) provides more details.

OpenADB-ALES multimission altimetry

To compare the XTRACK-ALES product with an analogous along-track dataset, which benefits from an extended number of missions, we use the OpenADB-ALES multimission dataset (available at <https://openadb.dgfi.tum.de/en/>). This 1Hz dataset is based on the missions ERS-2, Envisat, Saral, Topex, Jason 1 to Jason 3, their extended missions and Sentinel 3A and 3B, which provide continuous altimetry time series of 25 years (1995-2020). For all missions, satellite orbits in the ITRF2014 are used. To reduce systematic differences between the different missions, the tailored altimetry data is cross-calibrated using the global multi-mission crossover analysis (MMXO) (Bosch and Savcenko, 2007, Bosch et al., 2014). The along-track data underwent an outlier analysis using absolute thresholds, scanning running mean standard deviations and rejecting extreme consecutive differences (please refer to Oelsmann et al., 2021). All the orbits and geophysical corrections and adjustment are documented in Oelsmann et al., 2021, as well. Note that the reference frame of this dataset (as used in this study) was updated to ITRF2014 (homogeneously for all missions) compared to Oelsmann et al., 2021 (ITRF2008). As discussed by WM16, different implementations of different ITRF releases can affect the resulting altimetry trends. The updated version contains now also the Sentinel missions and Topex.

CMEMS gridded altimetry

To discover the differences between the dedicated coastal along-track altimetry data with gridded data, we investigate the performance of the previous vDT2014 C3S altimeter gridded sea level product consisting of monthly, SLAs with a spatial resolution of 0.25° . As mentioned by Kleinherenbrink et al., 2018, this multimission dataset features a latitude-dependent spatial interpolation with scales in the order of 50-300 km (Ducet et al., 2000). Note, that from 15/05/2017 this dataset is temporally extended by the vDT2018 dataset. The product was obtained from <https://www.aviso.altimetry.fr>.

PSMSL tide gauges

The monthly mean TG data are obtained from the datum-controlled PSMSL (Holgate et al., 2013) database. The service undertakes quality control of the data including checks for consistency of the annual cycle, outlier detection and intercomparisons with neighbouring stations, which enhances the reliability of the data. We select those TGs, which contain at least 180 months (15 years) of valid measurements during the altimetric era (1993/01-2020/12), resulting in a total of 691 stations. We apply the same monthly averaged DAC correction as used for the CMEMS data (Carrère and Lyard, 2003) from the closest point. To account for potential long-period tides we subtract the same tidal correction as applied for the SLA data (FES2014).

As an alternative to the monthly TG observations, one could also use high frequency (i.e., hourly) TG observations from the GESLA dataset (Woodworth et al., 2016). However, GESLA contains only data up to 2015, which severely limits the considered period of observations. Moreover, there is no quality check applied to GESLA, in contrast to PSMSL. Thus, for the purpose of generating robust SAT-TG VLM



estimates, we decide to use as many data as possible and restrict the TG selection to the monthly PSMSL data.

GIA datasets

We use the GIA solution from Caron et al., 2018 (hereinafter called C18), which is based on 128,000 forward models. The likelihood of parameters, which describe the Earth structure and ice history was estimated from an inversion of GPS and relative sea level data within a Bayesian framework. The GIA estimate represents the expectation of the most likely GIA signal. Formal uncertainty estimates were directly inferred from the Bayesian statistics. We emphasize that the GIA estimate does not capture any other more regional or local VLM processes (e.g., such as tectonic activity) and has therefore a limited validity as a validation basis of VLM.

GNSS datasets

The GNSS time series are obtained from the Nevada Geodetic Laboratory (NGL) of the University of Nevada (Blewitt, et al., 2016; <http://geodesy.unr.edu>, accessed on 1 September, 2020). We only use time series with minimum lengths of 5 years and with at least 4 years of valid observations. Additionally, based on the uncertainty estimates provided by MIDAS, we reject GNSS time series with a trend uncertainty larger than 1.5 mm/year. This prevents us from using very noisy GNSS data. Finally, we select the closest GNSS station within a 50 km and 1 km radius to a TG, to compare the influence of potentially local VLM variation on the comparability.

The altimetry datasets feature different corrections, adjustments, missions and reference frames which can contribute to different solutions of SAT-TG VLM data. Thus, we emphasize the key differences among used datasets in the discussion of the results.

2.1.2. Methods and algorithm description

Coupling of altimetry and TG data

Before combining altimetry and TG data, we compute monthly averages of the XTRACK-ALES and OpenADB-ALES along-track data at every point on the track, to obtain homogeneous temporal sampling.

Next, in order to couple the SLA data with the TG observations, we investigate different strategies. We particularly focus on the approach put forward by Kleinerherenbrink et al., 2018 and Oelsmann et al., 2021. Here, we select SLA anomalies from a larger coastal region in the vicinity of the TG. The SLA are selected by computing statistics like the correlation, the rms or the residual annual cycle (hereinafter called AC) between every time series on the track and the TG time series, using a maximum radius of 300 km around the TG. Both the SLA and TG time series are detrended and deseasoned before computing the statistics. We then select 20% of the best performing SLAs according to these statistics. The selected region represents the Zone of Influence (ZOI), i.e. the region where SLA are in high agreement with the TG observations. In contrast to selecting a single point (e.g. the point of highest correlation, PoHC) this approach has the advantage that potentially multiple tracks are selected and a better temporal sampling is achieved.

The set of the 20% best performing (non-detrended and non-deseasoned) SLAs is spatially averaged and subtracted from the monthly TG observations to obtain the VLM time series. As an alternative to the ZOI (using the cor, rms and AC statistics) we select the PoHC and the closest point (hereinafter called 'closest') of observation. VLM is only computed based on time series which have a minimum length of 10 years. In this work no manual screening (and possible rejection) of the resulting VLM time series is applied.

In section 2.2 we also compare a gridded altimetry product (CMEMS) with the along-track datasets. The VLM SAT-TG of this gridded dataset are also based on the ZOI, which is itself based on the 20% highest correlated grid points within a radius of 300 km. Given the 50 - 300 km interpolation radius of this dataset, SLAs within the ZOI can potentially contain information of SL beyond this maximum radius of 300 km.



Trend and uncertainty computation

In order to detrend and deseason the data we subtract a linear regression model consisting of offset, a linear trend as well as annual- and semi-annual components (using harmonic functions).

To compute the final VLM and uncertainties we use Maximum Likelihood Estimation by fitting the data to the same deterministic model, as described above. The noise is approximated with a power-law (PL) plus white noise (WN) model, which accounts for autocorrelation in the data and thus provides a more accurate estimation of the trend uncertainties. This noise model combination was often applied in literature for VLM from SAT-TG or GNSS time series (see, e.g., Santamaria-Gomez et al., 2011, WM16, Kleinherenbrink et al., 2018, Oelsmann et al., 2021). We estimate the fraction of the WN and the PL noise, as well as the driving noise, which scales the combined estimated noise components. Moreover, a spectral index d is estimated, which determines the characteristics of the PL noise process, more precisely, the dependence of the variance of the noise on frequencies. Here, a spectral index of $d = 0$ would be equivalent to WN, a spectral index of $d = 0.5$ is equivalent to Flicker Noise and an index of $d = 1$ would describe Brownian motion. Thus, the higher the index, the more power has the variance of the noise at low frequencies, which substantially impacts on the magnitude of estimated trend uncertainties. We use the Hector software to compute these statistics (Bos et al., 2013).

2.2. Validation results

2.2.1. Comparison of different data-selection approaches: XTRACK - PSMSL

Combination of monthly TG and along-track data

Figure 1 and Figure 2 exemplify the spatial correlations, which are computed based on monthly averaged XTRACK_ALES along-track data and PSMSL TG observations. For the North East Atlantic region, we observe strong differences in the spatial correlation pattern. For example, correlations are much higher and much more homogeneous in the North Sea shelf-sea region, than off the Portuguese coast, where the shelf is relatively narrow. This indicates an influence of bathymetry on SL variations and thus on the correlation pattern of SLAs with TG observations, as also shown by Oelsmann et al., 2021. We emphasize that the correlations are also generally influenced by both the data quality of altimetry and TGs.

In Figure 2, which shows some regional examples, one can also observe that in some cases, the closest SLAs show reduced correlations compared to, for instance, the ZOI selection (which is highlighted by blue borders of the altimetry data).

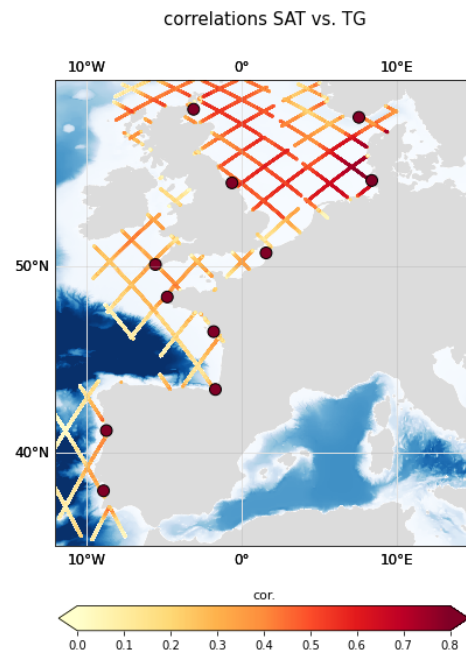


Figure 1: *Along-track correlations based on monthly PSMSL and XTRACK-ALES data for selected stations. Correlations are computed with respect to the nearest TG within a radius of 300 km (in the zone of influence). Note, that some of the correlations of two neighbouring TG stations might overlap in this figure. The blue shading indicates the bathymetry.*

We show the associated SLA time series (altimetry and TG) of the three examples of Figure 2 as well the differences in Figure 3. The time series, which are based on the ZOI and the cor and rms statistics, agree well with the TG observations on monthly, annual and interannual time scales. Both time series (ZOI-cor, ZOI-rms) are also very similar to each other. The time series based on the PoHC deviates



more from the TG observation in all three examples. Here, the differences w.r.t. TG are almost twice as large as the ones derived from the ZOI-cor or ZOI-rms statistic (-10 cm noise amplitudes vs. 5 cm).

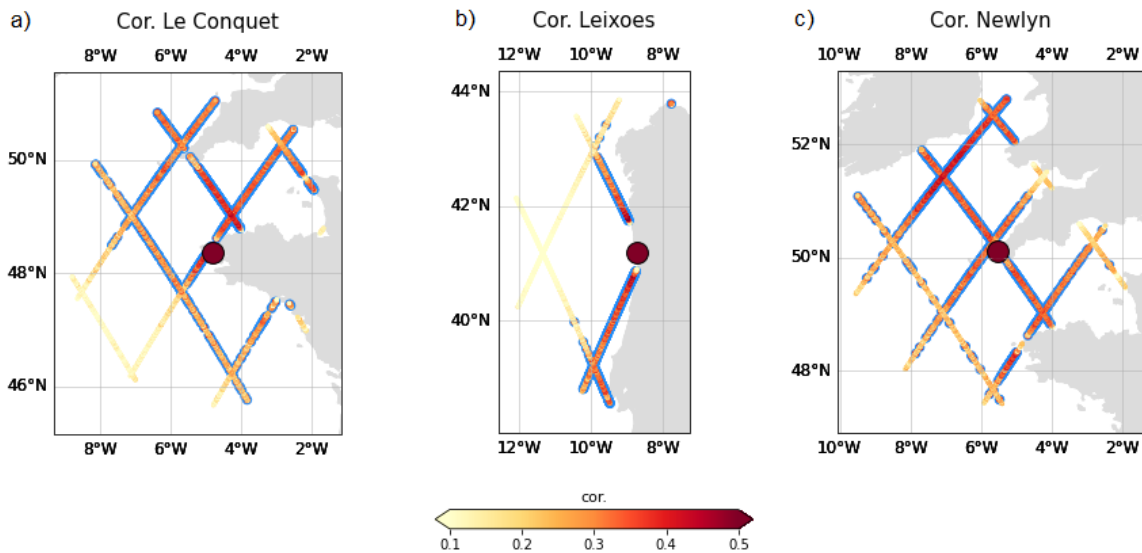


Figure 2: *Along-track correlations based on monthly PSMSL and XTRACK-ALES data. The 20% best correlated points are highlighted with blue borders.*

Better consistency of the ZOI-cor and ZOI-rms time series with TGs w.r.t to the PoHC selection, could be caused by the higher temporal density of the data, which were combined in the ZOI. Here, as shown in Figure 2, multiple tracks are selected, which provides more observations within a single month. Thus, the monthly ZOI time series might fit better to the TG based on the PoHC.

2.2.1.1. XTRACK-ALES - PSMSL Comparison of the statistics: cor, rms, AC, closest, PoHC

Table 1: Summary of statistics of the combination of monthly XTRACK-ALES and PSMSL data for all regions and available TGs. We show the median of correlations, VLM trends and uncertainties, as well as the median driving noise and the spectral index.

	cor	rms	AC	closest	PoHC
Correlation	0.779	0.755	0.735	0.287	0.621
Trend [mm/year]	-1.652	-1.492	-1.493	-1.176	-1.598
Trend uncertainty [mm/year]	1.019	0.964	1.133	3.176	0.998
Driving noise [mm]	25.875	25.735	27.397	95.781	55.554
Spectral index	0.260	0.260	0.290	0.159	0.042
Count	253	253	253	244	253

Figure 4 and Table 1 show the geographical distribution and average statistics of the correlations of SAT SLAs with TG observations. The statistics are given for 253 TGs, except for the criterium 'closest', where only 244 results are shown. Note, that for this selection some of the time series are shorter than 10 years, and thus do not pass this minimum length requirement. The SAT SLAs are computed for the different selection criteria and are detrended and deseasoned. The time series which are based on the ZOI selection (cor, rms, AC) score with the highest correlations, with median correlations of almost 0.8. Here, the ZOI-cor selection slightly outperforms the other criteria. Interestingly, the correlations derived from the averaged SLA in the ZOI also outperform the correlations when only



single along-track time series, i.e., the PoHC are used (median ~ 0.6). This further substantiates the assumption, that higher temporal density might play an important role for the ZOI-based time series.

The increased correlations of the ZOI time series (w.r.t. PoHC) are also in accordance with the time series in Figure 3, where the PoHC shows lower agreement with the TG observations. The selection based on the closest point provides substantially worse results than all the other selection criteria; it contains even negatively correlated data.

Differences in the correlation are also reflected in the associated trend uncertainties of the SAT-TG VLM (see Figure 5). We observe larger uncertainties particularly at the English coastlines, in northern Malaysia and India. Trend uncertainties are largest for the closest point selection. The trend uncertainties are all in the order of 1 mm/year (given as one sigma uncertainties) for the ZOI-cor, rms and AC as well as for the PoHC selection criteria. Thus, even though the correlations are reduced for PoHC (w.r.t. the ZOI time series) the trend uncertainties are still of similar magnitude. This is mostly caused by the larger amount of low frequency noise in the ZOI time series as indicated by the larger spectral indices, see Table 1 and Figure 7. Still, the driving noise (Figure 6), which scales the white and power law noise fractions is almost twice as large for the PoHC selection, as expected from the visual inspection of time series in Figure 3 and shown in Table 1. The driving noise indicates that the scatter of the data (or the standard deviations) is almost twice as large for the PoHC time series as compared to the ZOI-cor time series. As noted by WM16, a high white noise amplitude (as is the case for the PoHC and the closest criteria) can mask the detection of low-frequency noise, which is also the case for these criteria due to the low spectral indices. This can lead to misinterpretation of the results in particular the low uncertainties found for the PoHC criterium, which yields much larger variance in the time series than the ones based on the ZOI-approach.

Figure 8 shows the resulting VLM. The VLM pattern, which are associated with the SAT selection criteria correlation, rms, AC and PoHC agree qualitatively well. VLM which is based on the closest selection criterium exhibits much stronger variations compared to the other criteria. We observe positive VLM at the Norwegian and Swedish coastlines and slight subsidence along the northern European coastlines (e.g., Germany, Netherlands, France and Spain), which is consistent with the large-scale signal from GIA. Subsidence is also indicated for most parts of the Australian Coast, with an increased spatial variability of VLM at the eastern coastlines. For the selected regions (Europe, parts of Africa, Asia and Australia) we detect a median VLM in the order of -1 mm/year for all dataset combinations

2.2.1.2. XTRACK-ALES - PSMSL Comparison of SAT-TG VLM and GNSS VLM

In order to objectively evaluate the accuracy of the SAT-TG VLM, we compare the trends with VLM from GNSS observations. Here, we assume that the GNSS estimate represents the ground truth of VLM at a specific location. While the coupling of SAT and TG data can have a strong effect on the VLM itself in the first place, also the coupling of GNSS and TG data can influence the comparability of SAT-TG and GNSS trends (see, e.g., Kleinherenbrink et al., 2018). VLM can be affected by very localized processes, for instance, at shorter distances (1-10 km), VLM can vary substantially (e.g., see WM16). Therefore, in this study we compare different allowed distances between TG and GNSS stations of 1 km and 50 km, to investigate and mitigate possible influences, stemming from local VLM variability. We emphasize that quality issues of GNSS VLM estimates can also cause a reduced consistency with SAT-TG VLM. Thus, further quality control of the data (in addition to the objective GNSS selection criteria), like manual screening, could additionally improve the agreement (WM16).

As we show in Figure 4 the SAT and TG data are not homogeneously correlated and have different noise levels, which leads to differing SAT-TG VLM uncertainties. Thus, we also investigate if an objective selection criterium can support the identification of flawed SAT-TG time series and trends. Here, we use a correlation threshold of 0.6, which is derived from the monthly SAT and TG timeseries. A correlation of 0.6 is equal to the lower 10 percentile of the time series based on the ZOI-cor criterion.

Figure 9 illustrates the scatter of the differences between SAT-TG and VLM. Here, we show the scatter depending on the different criteria (correlation threshold of 0.6 and GNSS - TG distance). The variance of SAT-TG minus GNSS VLM reduces drastically, when stations with a maximum distance of 1 km are combined (compared to a distance of 50 km). However, as shown in Table 2 this also strongly



reduces the number of TG-GNSS pairs. Figure 9 illustrates that the median bias of SAT-TG VLM, as well as the scatter is lowest for the time series derived from the ZOI approach.

Table 2 lists the RMS of trend differences as well as the median bias of SAT-TG VLM w.r.t. GNSS VLM. The lowest RMS of trends (for $\text{cor} > 0.6$ and distance = 1 km) is obtained for the ZOI-rms, ZOI-AC and ZOI-cor criteria (1.48, 1.47 and 1.50). The RMS for the PoHC criterium is 1.76. For all criteria and all outlier selection criteria the SAT-TG VLM are biased against the GNSS in the order of approximately -0.5 mm/year, which also increases the RMS of trend differences.

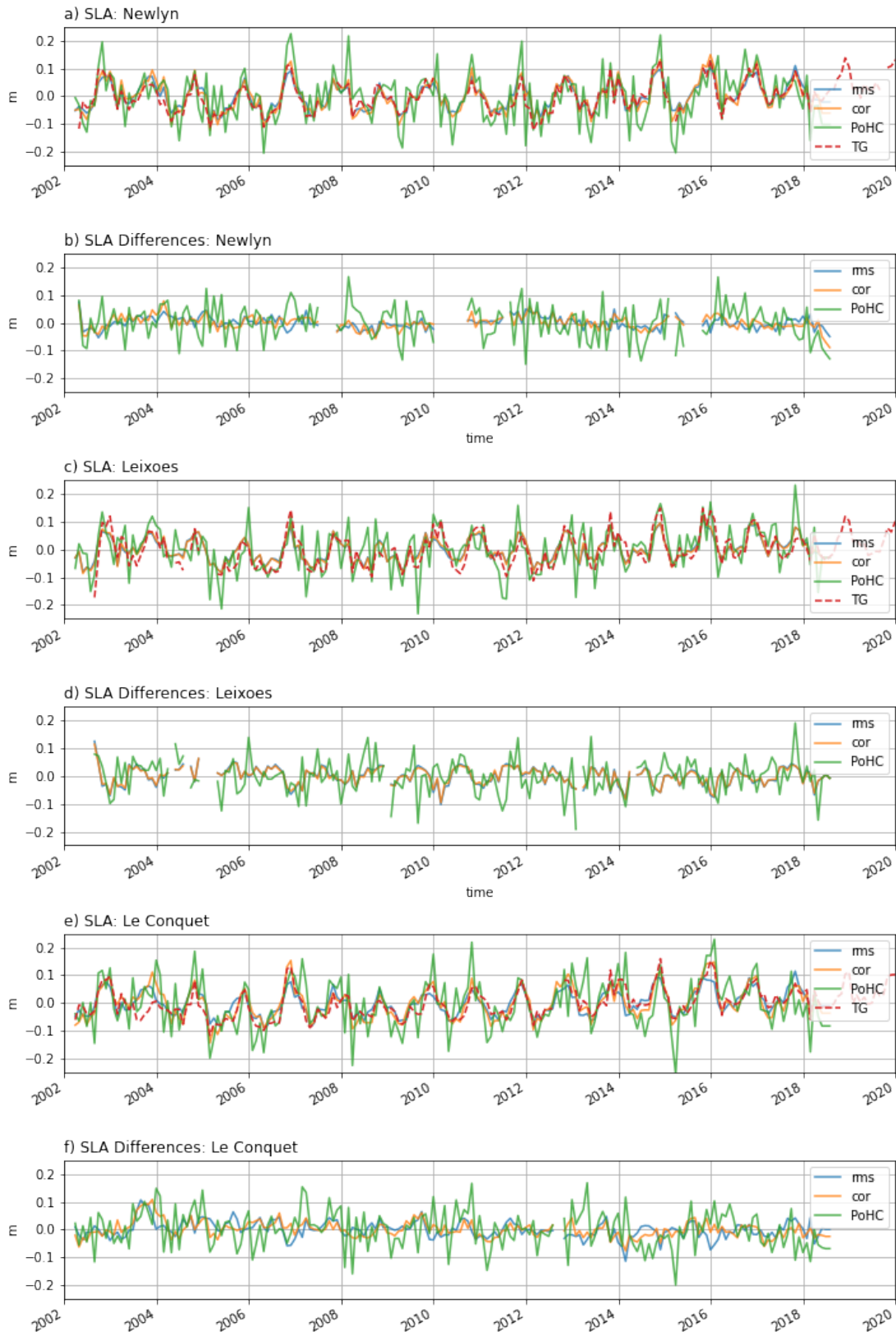


Figure 3: Shown are SLA time series of altimetry and TG data as well as the differences of SLAs for selected stations and different coupling criteria: rms, cor and PoHC. Note, that the closest point is not shown, due to the larger discrepancies of the TG and altimetry data for this selection.

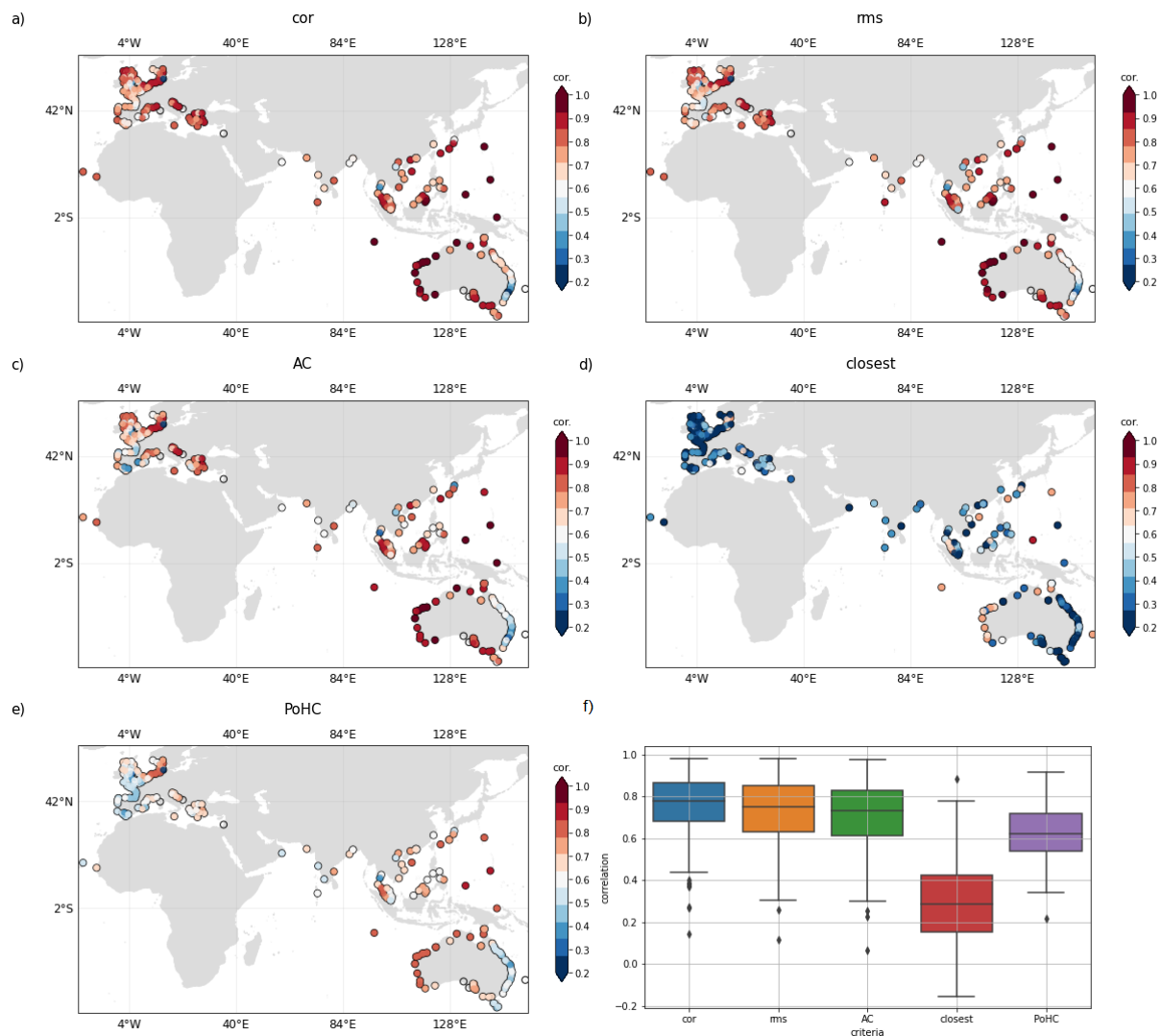


Figure 4: Correlations of monthly SAT and TG (PSMSL) observations (both detrended + deseasoned). The SAT SLA time series are computed based on the different criteria: (a-c) 20% best correlations, rms or residual annual cycle, the closest point (d), as well as the point of highest correlation (e). The boxplot (f) shows the distribution of correlations (the median and lower and upper quartile ranges).

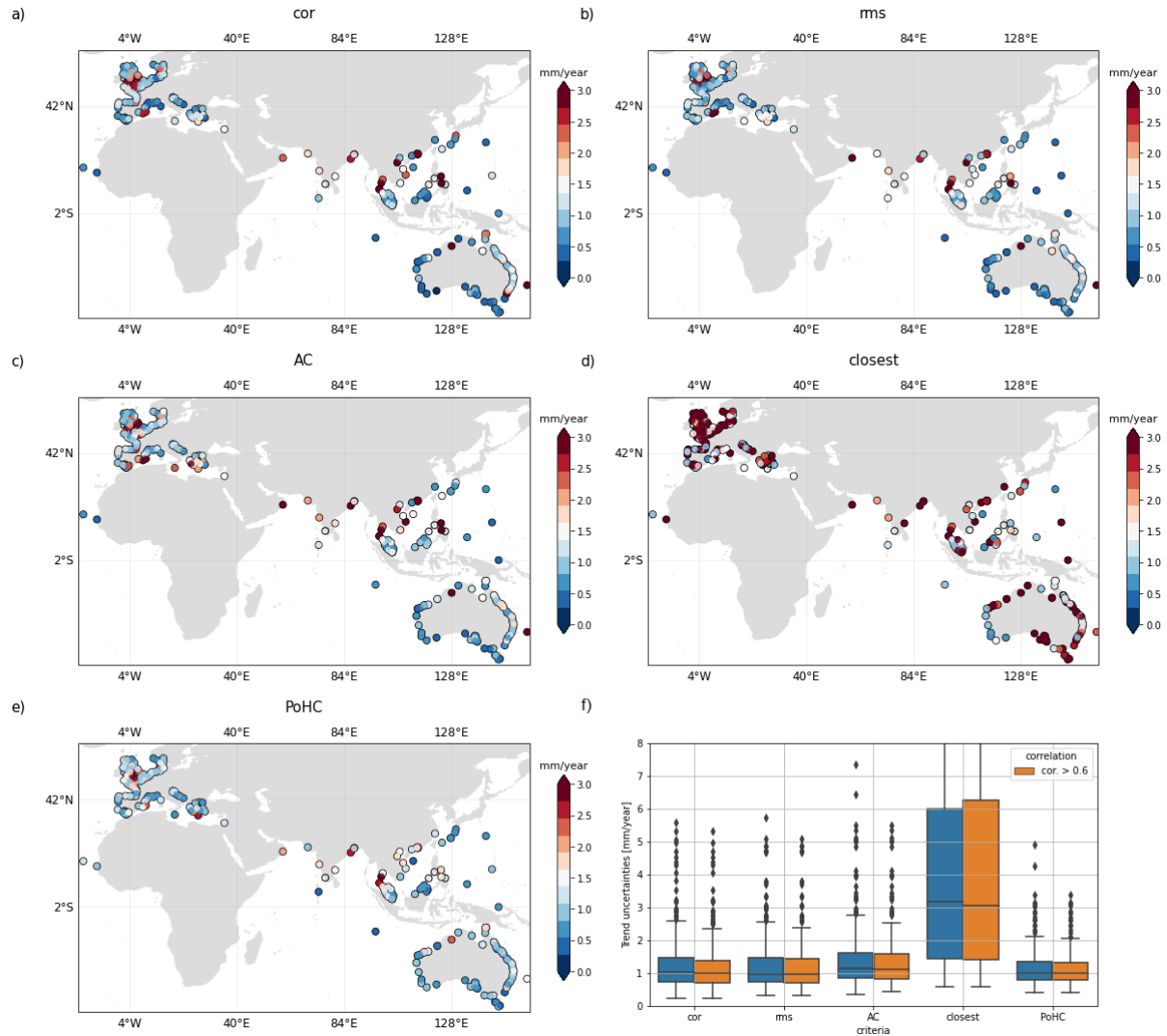


Figure 5: *Trend uncertainties (mm/year) of SAT-TG VLM. VLM is computed based on the different criteria: (a-c) 20% best correlations, rms or residual annual cycle, the closest point (d), as well as the point of highest correlation (e). The boxplot (f) shows the distribution of trend uncertainties (the median and lower and upper quartile ranges). In (f) we additionally show the results (orange), in case a correlation threshold of 0.6 is applied (based on the correlations of the time series based on the ZOI + cor criterium with monthly TG data).*

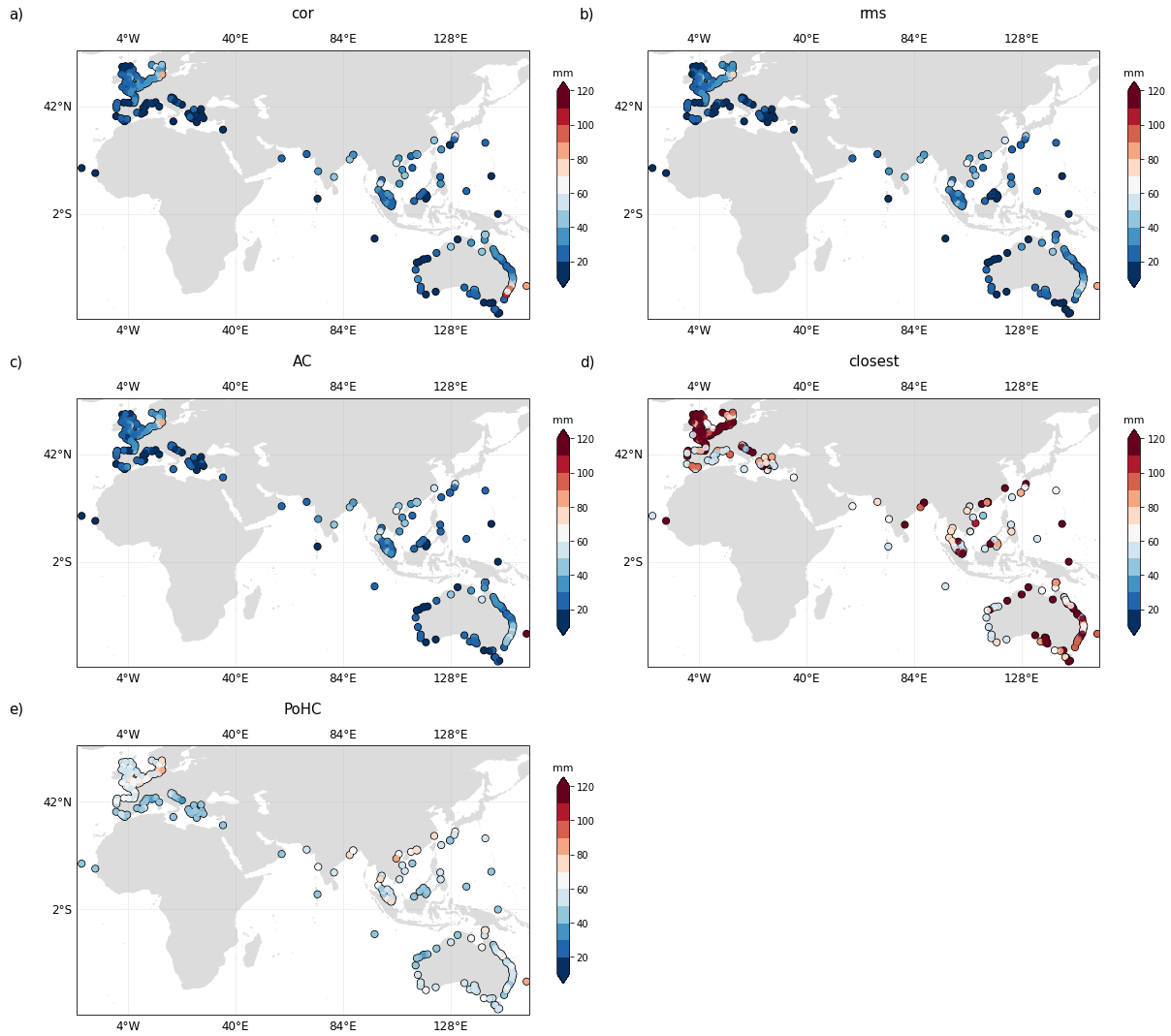


Figure 6: Driving noise (mm) of SAT-TG VLM. VLM is computed based on the different criteria: (a-c) 20% best correlations, rms or residual annual cycle, the closest point (d), as well as the point of highest correlation (e).

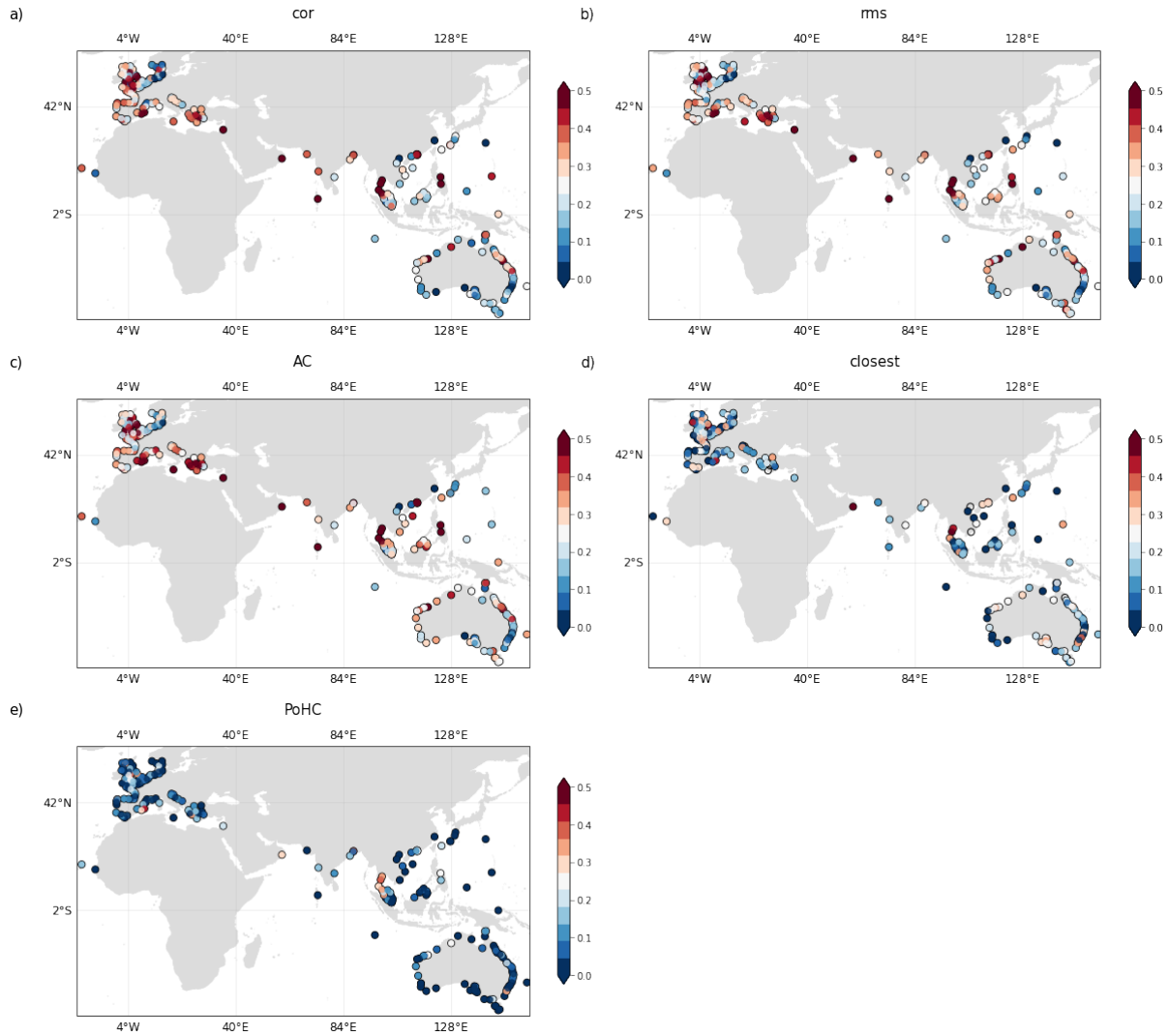


Figure 7: Spectral index of SAT-TG VLM. VLM is computed based on the different criteria: (a-c) 20% best correlations, rms or residual annual cycle, the closest point (d), as well as the point of highest correlation (e).

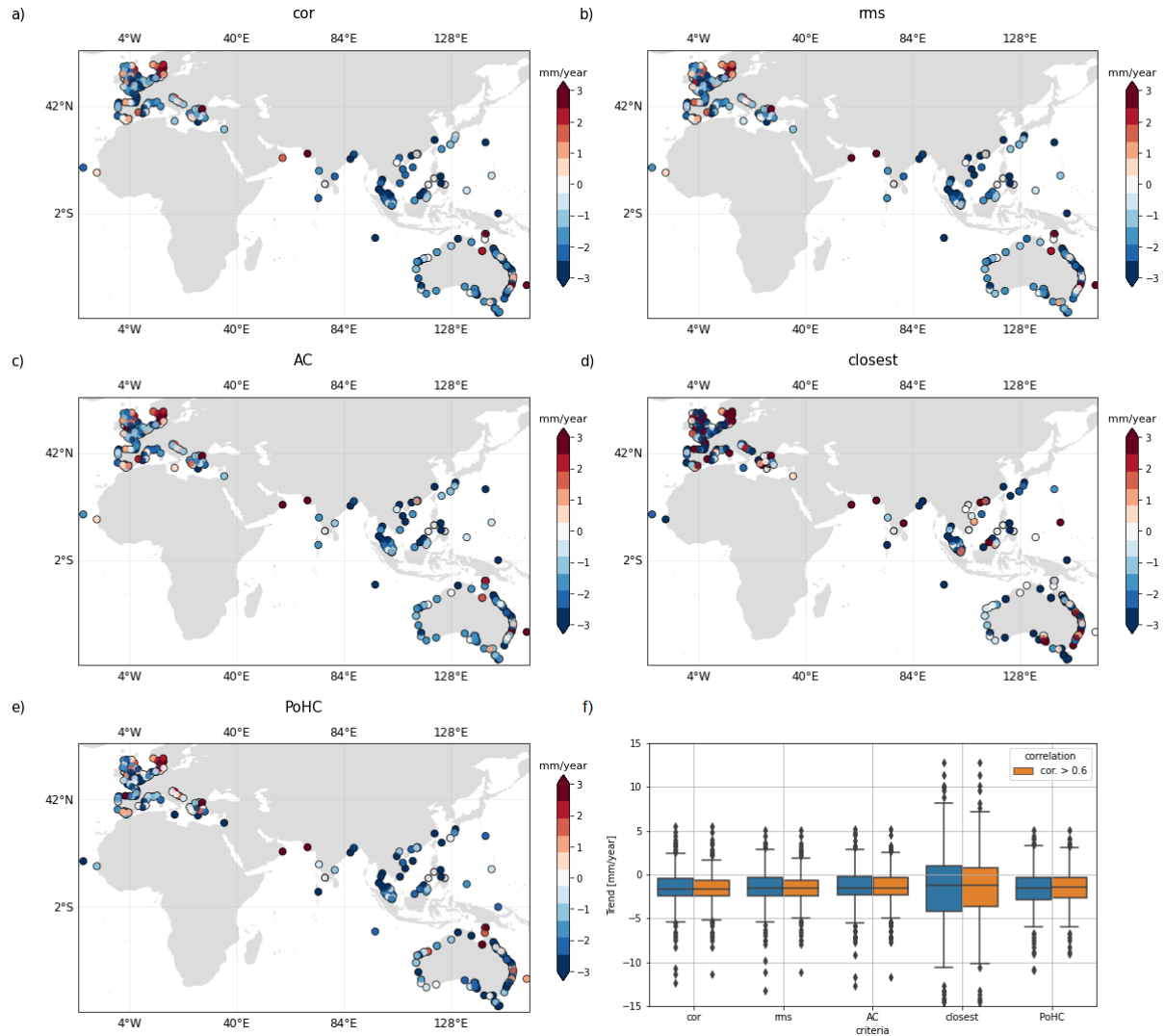


Figure 8: Trends (mm/year) of SAT-TG VLM. VLM is computed based on the different criteria: (a-c) 20% best correlations, rms or residual annual cycle, the closest point (d), as well as the point of highest correlation (e). The boxplot (f) shows the distribution of trends (the median and lower and upper quartile ranges). In (f) we additionally show the results (orange), in case a correlation threshold of 0.6 is applied (based on the correlations of the time series based on the ZOI + cor criterium with monthly TG data).

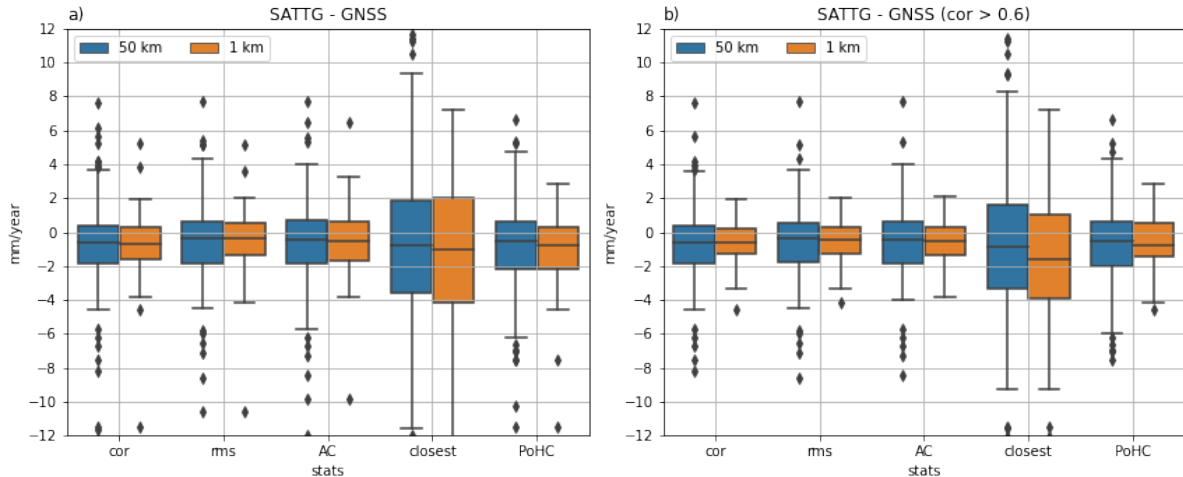


Figure 9: Boxplots of differences of SAT-TG VLM (XTRACK-ALES - PSMSL) and GNSS VLM. The data are grouped according to the distance between TG and GPS station, as well as a correlation threshold of 0.6. The correlation threshold is based on the XTRACK-ALES and TG data (ZOI-cor criterium).

The results (Table 2) show first of all, that the application of the ZOI is also supported by the comparisons of SAT-TG VLM with GNSS data. Secondly, using an absolute correlation threshold can substantially improve the consistency of SAT-TG and GNSS VLM (e.g., 36% or 0.81 mm/year reduction in RMS, for ZOI-rms and distance = 1, compared to no correlation threshold). Finally, it is also crucial to only use stations which are closely located to each other. In summary, the RMS for the best selection is in the order of magnitude of the RMS of SAT-TG and GNSS differences from WM16 (1.47 mm/year), who used gridded altimetry data (CMEAS, previously called AVISO). Nevertheless, the RMS is still larger as in Kleinherenbrink et al., 2018 (1.22 mm/year). In their study a different dataset based on Topex, Jason 1 and 2 from the RADS database (Scharroo et al., 2012) spanning the period 1993 and 2015 was used. Thus, the different time periods considered and different validation settings (in particular, GNSS-TG coupling) hinder an objective comparison. In section 2.2.3.1 we will further discuss the origins of the trend bias and its influence on the agreement with GNSS data.

Table 2: Comparison of SAT-TG VLM (XTRACK-PSMSL) and GNSS VLM. Shown are the RMS of trends and the median bias of differences for all data (as well as for a sub-selection with a correlation threshold of 0.6). The correlation threshold is based on the XTRACK-ALES and TG data (ZOI-cor criterium).

distance	Statistic	cor > 0.6	all	cor > 0.6	all	cor > 0.6	all
		RMS [mm/year]	RMS [mm/year]	median [mm/year]	median [mm/year]	count	count
1 KM	AC	1.471	2.266	-0.506	-0.490	45	54
	PoHC	1.767	2.606	-0.772	-0.812	45	54
	closest	5.525	5.569	-1.306	-0.974	44	53
	cor	1.503	2.377	-0.614	-0.656	45	54
	rms	1.448	2.250	-0.405	-0.389	45	54
50 KM	AC	2.164	2.471	-0.467	-0.438	170	199
	PoHC	2.454	2.719	-0.518	-0.637	170	199
	closest	5.379	5.396	-0.774	-0.725	166	195
	cor	2.226	2.564	-0.607	-0.613	170	199
	rms	2.169	2.482	-0.397	-0.390	170	199



2.2.2. XTRACK-ALES - PSMSL Comparison with GIA models

Next to the GNSS data, we compare the SAT-TG VLM to an estimate of GIA from Caron et al., 2018. Here, we combine the SAT-TG VLM with the closest available grid point of the GIA product. We also account for surface deformation due to mass changes, which are generated e.g., by ice mass changes or surface water loading changes. We use data of ‘contemporary mass redistribution’ (CMR) provided by Frederikse et al., 2020.

As demonstrated by the larger RMS values in Table 3, the GIA estimate does not represent an ideal validation basis of SAT-TG VLM, as compared to the GNSS dataset. Of course, more localized VLM e.g., tectonic activity, human influences or nonlinear surface deformation are not captured by the GIA model. Thus, the RMS of SAT-TG and VLM trends is increased w.r.t. GNSS validation results. Adding information of CMR to the GIA trends, slightly improves the RMS (on average for all selection criteria). However, the best RMS value of 2.44 mm/year (as obtained for the ZOI-rms criterium and a correlation threshold > 0.6) is still much larger compared to the result of the GNSS validation. Another reason why using a GIA model to investigate the performances of SAT-TG VLM for the selected TG stations might not be the best choice for this current dataset, might be the fact, that the overlap of the regions with the strongest GIA signal (Scandinavia, North America) and the TG locations is very limited. Hence, extending the XTRACK-ALES dataset to regions, where GIA has a stronger impact, could contribute to the investigations of the associated VLM.

Table 3: Comparison of SAT-TG VLM (XTRACK-PSMSL) and GIA (+CMR) VLM. Shown are the RMS of trends and the median bias of differences for all data (as well as for a sub-selection with a correlation threshold of 0.6). The correlation threshold is based on the XTRACK and TG data (ZOI-cor criterium).

VLM model	Statistic	cor > 0.6	all	cor > 0.6	all	cor > 0.6	all
		RMS [mm/year]	RMS [mm/year]	median [mm/year]	median [mm/year]	count	count
GIA	AC	2.464	2.600	-1.294	-1.242	220	253
	PoHC	2.626	2.838	-1.325	-1.424	220	253
	closest	5.289	5.294	-0.980	-0.996	211	244
	cor	2.476	2.647	-1.376	-1.345	220	253
	rms	2.445	2.588	-1.280	-1.213	220	253
GIA + CMR	AC	2.409	2.593	-1.251	-1.179	220	253
	PoHC	2.609	2.828	-1.347	-1.383	220	253
	closest	5.298	5.313	-1.044	-0.975	211	244
	cor	2.456	2.662	-1.304	-1.277	220	253
	rms	2.402	2.591	-1.211	-1.132	220	253



2.2.3. Comparison with other altimetry datasets

The XTRACK-ALES SAT-TG VLM are compared with SAT-TG VLM estimates of the along-track OpenADB-ALES product and the CMEMS product. The main rationale of this analysis is to shed light on how the addition of more missions or how gridding of the data might influence the SAT-TG performances. The performances are again evaluated by means of the comparison with GNSS estimates and the formal SAT-TG VLM uncertainties.

Table 4 provides a summary of the comparison with GNSS VLM data. Next to the RMS, we also computed the standard-deviation of trends which is not affected by potential trend biases. We repeated the analysis as before (distance and correlation threshold). In the following, we only refer to the data based on $\text{cor} > 0.6$ and distance = 1 km, as this provides the best agreement w.r.t. GNSS VLM.

The RMS of XTRACK-ALES and OpenADB-ALES is of similar magnitude (1.5 and 1.53 mm/year); CMEMS has the lowest RMS w.r.t. GNSS data (1.33). As shown in Figure 10, the VLM of all three altimetry datasets have very different biases with respect to each other. For example, most of the OpenADB-ALES VLM is by approximately 1 mm/year larger than the VLM based on XTRACK-ALES. Larger VLM, which is derived from with SAT-TG method, means larger absolute sea level trends, i.e., higher trends observed by altimetry (when the same TG data are used). The bias w.r.t. GNSS is 0.86 mm/year for OpenADB-ALES and -0.61 mm/year XTRACK-ALES.

VLM trend biases also affect the RMS of the XTRACK-ALES and OpenADB-ALES data, as demonstrated by the much lower standard-deviations of VLM differences. The standard-deviation of VLM differences is lowest for the OpenADB-ALES, and very similar for CMEMS and XTRACK-ALES. Possible sources of trend biases are discussed in the next sub-section.

While the standard-deviations of the VLM differences agree relatively well, there are differences in the median formal uncertainties. These are 1.02 mm/year, 0.88 mm/year and 0.62 mm/year, for the XTRACK-ALES, OpenADB-ALES and CMEMS products. This substantiates, that both, the addition of missions, as well as time-space interpolation of the data (as done in the CMEMS product), increase the agreement of SAT and TG observations, which leads to a reduction in the residuals and thus an improvement of trend uncertainties of the associated SAT-TG VLM time series.

Table 4: Comparison of GNSS VLM with SAT-TG VLM which are based on the XTRACK-ALESS (ZOI-cor), CMEMS (ZOI-cor), OpenADB-ALES (ZOI-cor) altimeter datasets and PSMSL TGs. Shown are the RMS, the standard-deviations and the median bias of VLM differences for all data, as well as for a sub-selection with a correlation threshold of 0.6. The correlation threshold is based on the XTRACK-ALES and TG data (ZOI-cor criterium).

Dist.	Name	cor > 0.6	all	cor > 0.6	all	cor > 0.6	
		RMS (STD) [mm/year]	RMS (STD) [mm/year]	median [mm/year]	median [mm/year]	count	count
1 km	OpenADB	1.530 (1.274)	1.964 (1.827)	0.857	0.866	45	54
	CMEMS	1.331 (1.344)	1.843 (1.854)	0.094	-0.218	45	54
	XTRACK	1.503 (1.351)	2.377 (2.266)	-0.614	-0.656	45	54
50 km	OpenADB	2.241 (1.934)	2.477 (2.241)	1.060	1.011	169	198
	CMEMS	2.027 (2.032)	2.259 (2.264)	0.094	-0.065	169	198
	XTRACK	2.208 (2.098)	2.552 (2.464)	-0.602	-0.607	169	198

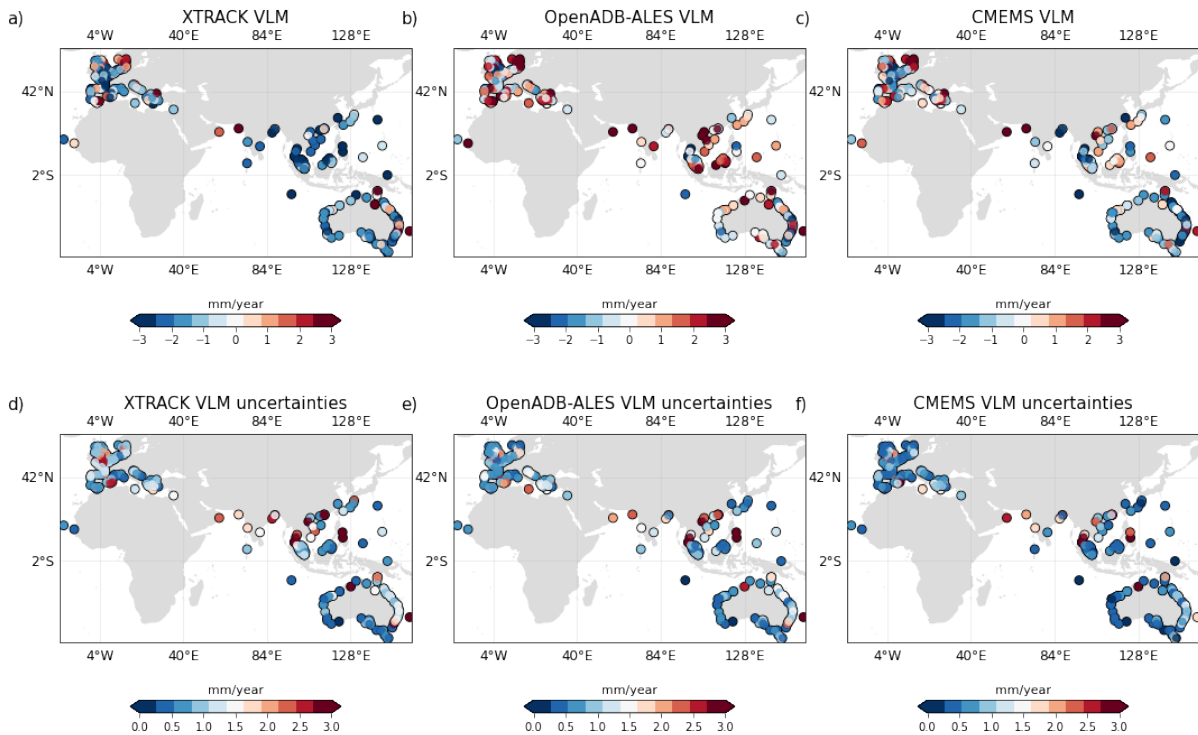


Figure 10: VLM (a-c) and uncertainties (d-e) for different SAT-TG combinations (XTRACK-ALES, OpenADB-ALES, CMEMS). For all datasets the ZOI-cor criterium to construct the SAT-TG time series was used.

2.2.3.1. Discussion of the altimetry trend biases

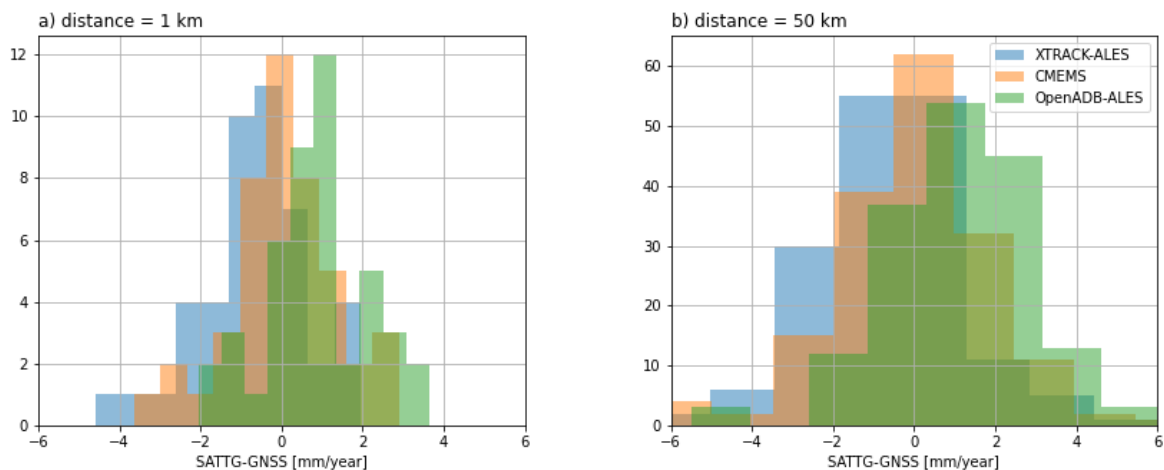


Figure 11: Histograms of trend differences (SAT-TG minus GNSS VLM) of the different altimetry dataset for different maximum allowed distances between TG and GNSS station: a) 1 km b) 50 km

Figure 11 illustrates that the distributions of the differences of VLM of the altimetry datasets are significantly shifted with respect to each other. The causes of these biases remain an open issue, which needs to be further investigated in future analyses. In the following, we discuss/exclude some



potential contributors of such trend biases, in particular referring to the differences between XTRACK-ALES and OpenADB-ALES.

First of all, the following corrections can be excluded as origins of trend biases, because they are used in both datasets, XTRACK-ALES and OpenADB-ALES: Range and sea state bias correction, wet troposphere (GPD+) and Ocean Tide (FES2014).

Other causes cannot be clearly excluded. For example, OpenADB-ALES uses a mix of DAC corrections. Here, the DAC correction as implemented in XTRACK-ALES (Carrere and Lyard, 2003) was only applied when the ECMWF ERA-Interim reanalysis (DAC-ERA; Carrère et al., 2016) was not available. OpenADB-ALES contains also more missions, in particular the ERS-2 + Envisat and the Sentinel missions. This does however not necessarily explain a trend bias, because the non-biased dataset CMEMS is also based on the ERS-2 + Envisat missions. We also find no significant change in the trend bias for OpenADB-ALES, when removing the Sentinel and TOPEX mission. Furthermore, the reference frame of the applied orbits could lead to trend biases. However, the comparison of two OpenADB-ALES multimission products, with different reference frames (ITRF2008 and ITRF2014) leads to a similar bias with respect to XTRACK-ALES for both cases. In contrast to XTRACK-ALES, OpenADB-ALES features a multi-mission calibration (MMXO) which reduces intermission biases and regionally coherent systematic errors, but does not feature a calibration against TG. Such a bias correction is not applied to the CMEMS dataset or XTRACK-ALES.

Also, the Ionospheric correction could cause trend differences. XTRACK-ALES's Ionospheric correction is based on GDR (From dual-frequency altimeter range measurement), OpenADB-ALES is based on the correction from NIC09 (Scharroo and Smith, 2010))

Finally, the GNSS station database itself influences the validation results of SAT-TG VLM. In case that VLM is not strictly linear over the considered period, GNSS (which are usually based on shorter time periods than SAT-TG) and SAT-TG might provide different trend estimates. This can, however, not explain the systematic differences between the altimetry based SAT-TG trends, which are computed over the exact same time periods. Thus, in summary, we highlight that the significant trend biases between the along-track products, which deteriorate the accuracy of the SAT-TG VLM as a whole (i.e. act as a constant trend-offset w.r.t. TG), require further investigations to be mitigated.

2.3. Dataset description

Table 5: Dataset description of the deliverable

DGFI_VLM_XTRACK_ALES_PSMSL_<critierium>_<vlm_version>_<sla_version>, consisting of point-wise VLM information derived from SAT-TG. We provide five different netCDF files, which contain VLM information for all applied SAT selection criteria (<critierium>). <vlm_version> refers to the dataset version and <sla_version> refers to the XTRACK-ALES SLA version number.

Dimensions:		
X = 253		
NetCDF coordinates/variables (dim): short_name	Description: long_name	Unit
lat(x)	latitude	degrees_north
lon(x)	longitude	degrees_east
psmsl_index(x)	Index of PSMSL TG	#



vlm_trend(x)	VLM trend based on SAT-TG over 2002-2018 (computed with PL-WN model)	mm/year
vlm_trend_unc(x)	VLM trend uncertainty (1 sigma) based on SAT-TG over 2002-2018 (computed with PL-WN model)	mm/year
spectral_index(x)	Spectral Index	
driving_noise(x)	Driving noise	mm
Global attributes:		
dataset_name	DGFI_VLM_XTRACK_ALES_PSMSL_<statistic>_<vlm_version>_<sla_version>	
description	Vertical land motion derived from altimetry and tide-gauge differences. Based on XTRACK-ALES (<sla_version>) and monthly PSMSL tide gauge data. Altimetry data are combined according to the <statistic> criterium. The ID of the deliverable is D1.2, associated algorithms and validation results can be found in D1.1.	
Authors	Julius Oelsmann, Marcello Passaro	
ID	D1.2	
Subcontractor	Technical University of Munich	
creation_time	Date + time	
version	v1	
Project_name :	SLCCI+; https://climate.esa.int/en/projects/sea-level	



3. D3 - Alt-TG VLM: Regional Map

The aim of task 1.3 is to derive a regularly-spaced coastline profile by spatial interpolation of sparse vertical land motion (VLM) data. The analysis takes into account VLM trend estimates and uncertainties, as computed in work-package D1.2. We use SATTG (altimetry minus tide gauge) trends (XTRACK/ALES dataset (v1.1, https://doi.org/10.5270/esa-sl_cci-xtrack_ales_sla-200206_201805-v1.1-202005), available at <https://catalogue.ceda.ac.uk/uuid/222cf11f49a94d2da8a6da239df2efc4>), which are combined based on the RMS (root-mean square error) statistic (see previous technical note D1.1). This dataset provides the best performances in terms of accuracy and uncertainty of the VLM (next to the dataset based on the correlation criterium).

3.1. Method

3.1.1. Data preprocessing - outlier rejection

We apply an objective outlier rejection as well as a manual inspection of VLM time series. With this approach we aim to reject time series which provide an impaired representation of the VLM signal. One major error source in the VLM time series are discrepancies between the tide gauge and the altimeter measurements, which are not fully alleviated in the combination procedure. Hence, we reject stations where the TG and altimetry time series (averaged in the Zone of Influence) have a correlation < 0.56 and where the driving noise of the VLM time series is above 0.42 mm. Both outlier-rejection statistics correspond to the 10th and 90th percentiles of the data. The definition of these thresholds is in agreement with those applied for the time series analysis in D1 (with the difference that we now also use the driving noise). Note that the driving noise was derived with Hector software (Bos et al., 2013) and provides information of the absolute noise amplitude in the data.

Not all of the problematic VLM time series can be identified with these objective criteria. Thus, we manually inspect the time series for irregular behavior, i.e., in particular abrupt jumps in the data. In this kind of data, discontinuities are most commonly generated by either physical ground motions which affect the TG vertical datum, or instrumental issues. The following two plots illustrate time series where discontinuities are found after manual inspection, as well as SATTG VLM time series which are rejected from the dataset.

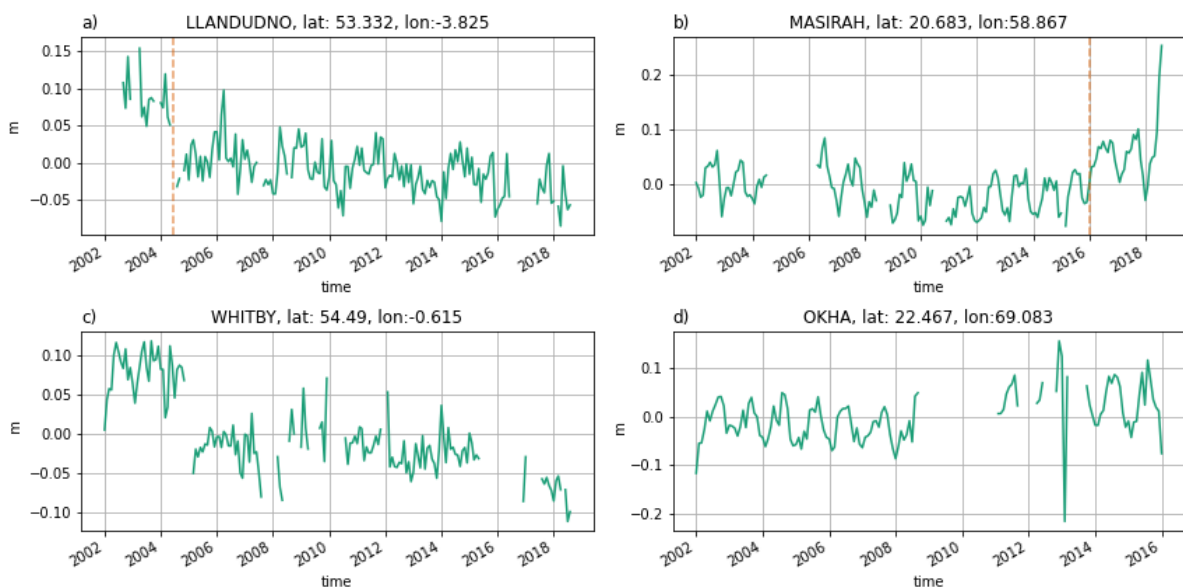


Figure 12: Problematic SATTG VLM time series, which are edited (a,b) or rejected (c,d) from the dataset. In a) the time series is truncated to the years 2005-2019, in b) the data after 2016 is rejected. Dashed vertical lines indicate possible discontinuities after manual inspection.



3.1.2. 2D interpolation - Transdimensional regression

Several previous studies focused on interpolating VLM, in particular to extrapolate VLM to areas where no direct VLM observations are available (e.g., Husson et al., 2018; Hawkins et al., 2019b; Hammond et al., 2021). Multiple 2D interpolation schemes have been applied, which include for instance ordinary Kriging, Spline interpolation, Radial Basis function interpolation, or Bayesian regression. A central issue of classical interpolation approaches is that they often rely on user assumptions of the correlation length scale (and thus the length scale of the weighting functions) of the VLM data. This length scale can however be variable, as it is influenced by the length scale of the VLM signals/processes, as well as by the actual distribution and availability of the data. For example, the spatial resolution of a VLM interpolation could be much higher in well instrumented regions such as central Europe, compared to Africa, or South America. Hence, we adopt the method developed by Hawkins et al., 2019b, which automatically estimates the level of smoothness (or the spatial resolution) of the data, based on the distribution as well as the formal uncertainties of the data. The Bayesian Transdimensional regression dynamically adapts the complexity (spatial resolution) of the interpolated surface and produces a full posterior distribution of the VLM data. The interpolated (VLM) surface is parametrized by a set of variable mobile nodes (grid points), onto which VLM values are assigned. The number of the nodes, which determine the complexity of the grid is an unknown parameter of the inversion and is itself estimated. Here, as in Hawkins et al., 2019b, we apply a Delaunay linear interpolation to recover a smooth surface. The posterior probability distribution of the unknown parameters is approximated using a hybrid of Markov chain Monte Carlo (MCMC) and Hamilton Monte Carlo techniques.

Prior to interpolation, we separate the VLM data into two macro-regions (Europe and Oceania + South Asia) as shown in the following plots. We run 56 independent Markov chains, which start from randomized initial conditions, which are drawn from the prior distribution of the parameters. Using synthetic data, Hawkins et al., 2019a showed that varying the number of chains (between 28 - 112 chains) does not have a significant impact on the posterior estimates. Hence, 56 chains are considered to be sufficient for this application. Every chain is run for 1,000,000 iterations where only the last 500,000 iterations are retained and averaged after thinning the models. At every iteration of the Markov chain, the model state is perturbed, which involves the variation of the number and distribution of the grid nodes. Thus, every Markov chain consists of a large ensemble of model states, which form the basis to compute the full posterior distribution. We use a discrete uniform prior between 1 and 1000 for the number of maximum used nodes, and a uniform prior of VLM rates between ± 10 mm/year. The final interpolated 2D map is projected onto a regularly space coastal profile of 0.1° resolution.



3.2. Results

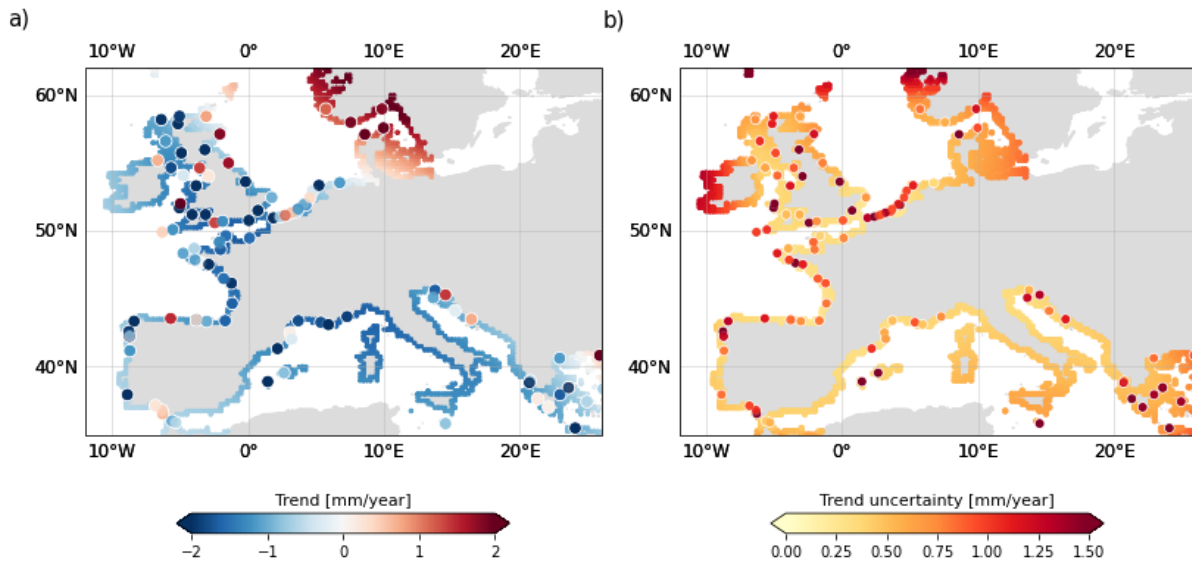


Figure 13: Continuous VLM (a) and uncertainties (b) along the European coastline. In addition to the continuous interpolated estimate, we show the SATTG VLM and uncertainties (white edge-colours).

In Figure 13 and Figure 14, we show the interpolated VLM for the two selected macro-regions. Next to the continuous VLM and uncertainty estimates, the SATTG VLM point estimates are shown. For the European continent (Figure 13), the estimates in the Baltic Sea are removed from the interpolation, due to the missing coverage of the XTRACK-ALES data in this area.

The interpolated VLM in Europe (Figure 13 and Figure 15a) shows an uplift signal towards Scandinavia, as well as subsidence between 1-2 mm/year in central and western Europe. The subsidence is linked to the known GIA fore-bulge collapse, e.g., see Peltier et al., 2015 or Caron et al., 2018. A high regional variability in the point-wise VLM rates along the English coastlines can be found, which is partly also associated with high formal uncertainties. This could be explained by the lower correlations of altimetry and TG in this region, which was also shown in the previous report of SL_cci (2020). The Bayesian regression incorporates the high formal uncertainties of the data and thus yields a smooth interpolated VLM surface in this area (with a spatial resolution of several hundred km), despite the high local variance of VLM.

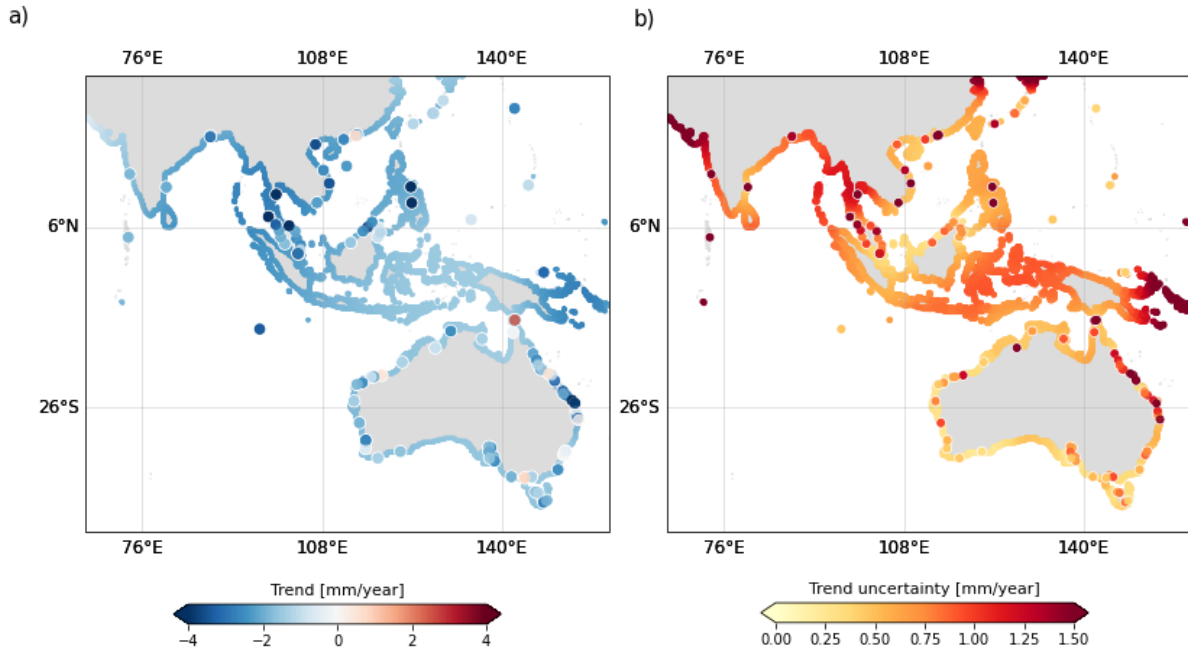


Figure 14: Continuous VLM (a) and uncertainties (b) on Oceania and South-East Asia. In addition to the continuous interpolated estimate, we show the SATTG VLM and uncertainties (white edge-colours).

Australia and the selected regions of South-East-Asia (SEA) are affected by subsidence between 0-2 mm/year (Figure 14 and Figure 15b). Similar as for the English coastline, the VLM and uncertainty point estimates have higher variance in areas that are associated with a lower correlation of altimetry and TGs. That particularly affects the North-Eastern Australian coastline, or the region north of Brisbane. Overall, the macro-region (SEA and Australia) has a very non-uniform distribution of SATTG data, with a much better coverage along the Australian coastline. This data distribution is well reflected by the interpolated uncertainties, which are higher in regions with low coverage and vice versa. The subsidence found for the Australian coastline, as well as the Philippines, for instance, are in accordance with previous research (Hammond et al., 2021, Hawkins et al., 2019b, Kleinherenbrink et al., 2018). This observed subsidence in Australia disagrees with VLM based on GIA (Hammond et al., 2021). This underlines the importance to utilize observed VLM to obtain continental-scale VLM processes unrelated to GIA.

Generally, it should be highlighted that the approach of interpolating SATTG VLM alone is still limited due to several reasons. A major problem is the relatively low coverage in some areas. For instance, regions like Italy, the Baltic region and large parts of Indonesia are not well covered in this work. Secondly, in particular the Philippines, as well as subduction zones (i.e., west of Sumatra) are affected by high spatial or temporal VLM variability (see Wöppelmann and Marcos, 2016 or Hammond et al., 2021), which cannot be represented by a smooth interpolated surface of linear VLM. Thus extending the database by adding GNSS observations and increasing the number of observations in time can strongly increase the robustness of the results and enhance the resolution VLM processes.

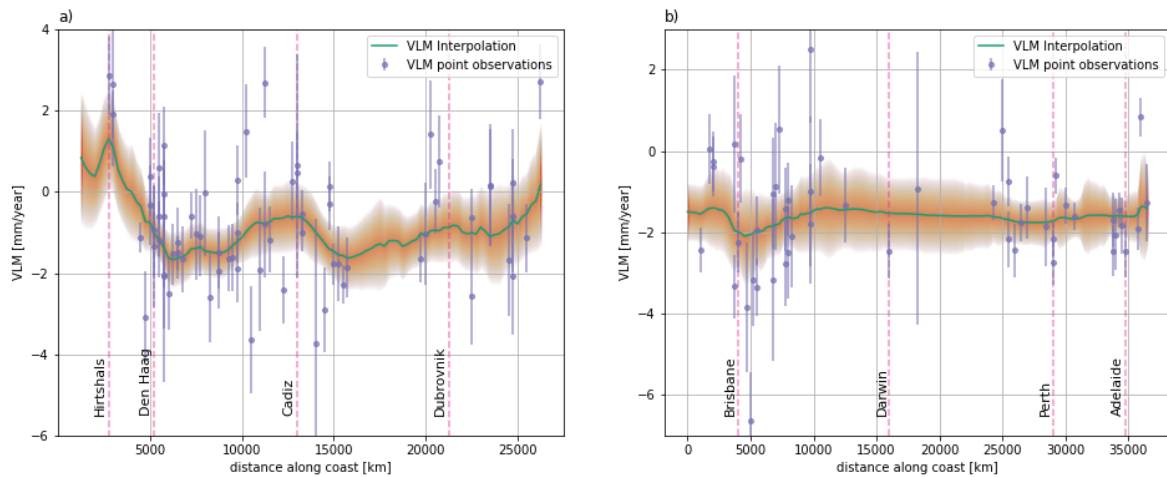


Figure 15: Continuous VLM and uncertainties along the European a) and the Australian b) coastline. The green line shows the posterior mean estimate, the orange shading encapsulates the 2-sigma confidence intervals of the interpolated VLM. SATTG VLM and uncertainties are shown in purple.

3.3. Dataset description

Table 6: Dataset description of the deliverable DGFI_2D_VLM_MAPS_XTRACK_ALES_PSMSL_RMS_v1_v1.1_202006, consisting of interpolated VLM data derived from SAT-TG.

Dimensions:		
X = 15708		
NetCDF coordinates/variables (dim): short_name	Description: long_name	Unit
lat(x)	latitude	degrees_north
lon(x)	longitude	degrees_east
region(x)	Macro-region over which interpolation is performed (Europe: 1; SEA_Australia: 0)	
vlm_trend(x)	Interpolated VLM trend based on SATTG over 2002-2018	mm/year
vlm_trend_unc(x)	Interpolated VLM trend uncertainty (1 sigma) based on SATTG over 2002-2018	mm/year
Global attributes:		
dataset_name:	DGFI_2D_VLM_MAPS_XTRACK_ALES_PSMSL_RMS_v1_v1.1_202006	
Description:	Vertical land motion derived from altimetry and tide-gauge differences. Point-wise VLM estimates are interpolated along the coastlines with Bayesian transdimensional regression for the macro-regions Europe and South-East-Asia/Australia (SEA_Australia). Based on the ESA SL_cci+ XTRACK/ALES dataset (v1.1, https://doi.org/10.5270/esa-sl_cci-xtrack_ales_sla-200206_201805-v1.1-202005), also available at https://catalogue.ceda.ac.uk/uuid/222cf11f49a94d2da8a6da239df2efc4 and monthly PSMSL tide gauge data.	



	Altimetry data are combined according to the RMS criterium. The ID of the deliverable is D3, associated algorithms and validation results can be found in D1.1.	
Authors	Julius Oelsmann, Marcello Passaro	
Project_name :	SLCCI+; https://climate.esa.int/en/projects/sea-level	
Subcontractor	Technical University of Munich	
creation_time	14-Feb-2022 12:45	
version	v1	

4. References

Florence Birol, Fabien Léger, Marcello Passaro, Anny Cazenave, Fernando Niño, Francisco M. Calafat, Andrew Shaw, Jean-François Legeais, Yvan Gouzenes, Christian Schwatke, Jérôme Benveniste, The X-TRACK/ALES multi-mission processing system: New advances in altimetry towards the coast, *Advances in Space Research*, Volume 67, Issue 8, 2021, Pages 2398-2415, ISSN 0273-1177, <https://doi.org/10.1016/j.asr.2021.01.049>.

Blewitt G, Kreemer C, Hammond WC, Gazeaux J (2016) Midas robust trend estimator for accurate gps station velocities without step detection. *Journal of Geophysical Research: Solid Earth* 121(3):2054-2068, DOI 10.1002/2015JB012552

Bos, M. S., Fernandes, R. M. S., Williams, S. D. P., and Bastos, L.: Fast Error Analysis of Continuous GNSS Observations with Missing Data. *J. Geod.*, 87, 351-360, <https://doi.org/10.1007/s00190-012-0605-0>, 2013.

Bosch, W., Dettmering, D., and Schwatke, C.: Multi-Mission Cross-Calibration of Satellite Altimeters: Constructing a Long-Term Data Record for Global and Regional Sea Level Change Studies, *Remote Sens.*, 6, 2255-2281, 2014.

Bosch, W. and Savcenko, R.: Satellite altimetry: Multi-mission cross calibration, in: *Dynamic Planet, International Association of Geodesy Symposia*, edited by: Tregoning P. and Rizos C., Vol. 130, Springer, Berlin, Heidelberg, https://doi.org/10.1007/978-3-540-49350-1_8, 2007.

Caron L, Ivins ER, Larour E, Adhikari S, Nilsson J, Blewitt G (2018) Gia model statistics for grace hydrology, cryosphere, and ocean science. *Geophysical Research Letters* 45(5):2203- 2212, DOI 10.1002/2017GL076644

Carrere, L., Faugère, Y., and Ablain, M.: Major improvement of altimetry sea level estimations using pressure-derived corrections based on ERA-Interim atmospheric reanalysis, *Ocean Sci.*, 12, 825-842, <https://doi.org/10.5194/os-12-825-2016>, 2016.

Carrère, L. and Lyard, F.: Modeling the barotropic response of the global ocean to atmospheric wind and pressure forcing - comparisons with observations, *Geophys. Res. Lett.*, 30, 1275, <https://doi.org/10.1029/2002GL016473>, 2003.

Cazenave, A., Dominh, K., Ponchaut, F., Soudarin, L., Cretaux, J. F., and Le Provost, C.: Sea level changes from Topex-Poseidon altimetry and tide gauges, and vertical crustal motions from DORIS, *Geophys. Res. Lett.*, 26, 2077-2080, <https://doi.org/10.1029/1999GL900472>, 1999.

Cipollini, P., Calafat, F. M., Jevrejeva, S., Melet, A., and Prandi, P.: Monitoring Sea Level in the Coastal Zone with Satellite Altimetry and Tide Gauges, *Surv. Geophys.*, 38, 33-57, <https://doi.org/10.1007/s10712-016-9392-0>, 2017.

Ducet, N., Le Traon, P. Y., and Reverdin, G.: Global high-resolution mapping of ocean circulation from TOPEX/Poseidon and ERS-1 and -2, *J. Geophys. Res.-Oceans*, 105, 19477-19498, <https://doi.org/10.1029/2000JC900063>, 2000.



Fernandes, M. J., Lázaro, C., Ablain, M., and Pires, N.: Remote Sensing of Environment Improved wet path delays for all ESA and reference altimetric missions, *Remote Sens. Environ.*, 169, 50-74, <https://doi.org/10.1016/j.rse.2015.07.023>, 2015.

Frederikse T, Landerer F, Caron L, Adhikari S, Parkes D, Humphrey V, Dangendorf S, Hogarth P, Zanna L, Cheng L, Wu YH (2020) The causes of sea-level rise since 1900. *Nature* 584:393-397, DOI 10.1038/s41586-020-2591-3

Hammond, W. C., Blewitt, G., Kreemer, C., & Nerem, R. S. (2021). GPS Imaging of global vertical land motion for studies of sea level rise. *Journal of Geophysical Research: Solid Earth*, 126, e2021JB022355. <https://doi.org/10.1029/2021JB022355>

Hawkins, R., Bodin, T., Sambridge, M., Choblet, G., & Husson, L. (2019a). Trans-dimensional surface reconstruction with different classes of parameterization, *Geochemistry, Geophysics, Geosystems*, 20. <https://doi.org/10.1029/2018GC008022>

Hawkins, R., Husson, L., Choblet, G., Bodin, T., & Pfeffer, J. (2019b). Virtual tide gauges for predicting relative sea level rise. *Journal of Geophysical Research: Solid Earth*, 124. <https://doi.org/10.1029/2019JB017943>

Holgate, S. J., Matthews, A., Woodworth, P. L., Rickards, L. J., Tamisiea, M. E., Bradshaw, E., Foden, P. R., Gordon, K. M., Jevrejeva, S., and Pugh, J.: New Data Systems and Products at the Permanent Service for Mean Sea Level, *J. Coastal Res.*, 493-504, <https://doi.org/10.2112/JCOASTRES-D-12-00175.1>, 2013.

L Husson, T Bodin, G Spada, G Choblet, C Kreemer, Bayesian surface reconstruction of geodetic uplift rates: Mapping the global fingerprint of Glacial Isostatic Adjustment. *Journal of Geodynamics*122, 25-40 (2018)

Kleinherenbrink, M., Riva, R., and Frederikse, T.: A comparison of methods to estimate vertical land motion trends from GNSS and altimetry at tide gauge stations, *Ocean Sci.*, 14, 187-204, <https://doi.org/10.5194/os-14-187-2018>, 2018.

Oelmann, J., Passaro, M., Dettmering, D., Schwatke, C., Sánchez, L., and Seitz, F.: The zone of influence: matching sea level variability from coastal altimetry and tide gauges for vertical land motion estimation, *Ocean Sci.*, 17, 35-57, <https://doi.org/10.5194/os-17-35-2021>, 2021.

Passaro, M., Cipollini, P., Vignudelli, S., Quartly, G. D., and Snaith, H. M.: ALES: A multi-mission adaptive subwaveform retracker for coastal and open ocean altimetry, *Remote Sens. Environ.*, 145, 173-189, <https://doi.org/10.1016/j.rse.2014.02.008>, 2014.

Peltier, W. R., Argus, D. F., & Drummond, R. (2015). Space geodesy constrains ice age terminal deglaciation: The global ICE-6G_C (VM5a) model. *Journal of Geophysical Research: Solid Earth*, 120, 450-487. <https://doi.org/10.1002/2014JB011176>

Pfeffer, J. and Allemand, P.: The key role of vertical land motions in coastal sea level variations: A global synthesis of multisatellite altimetry, tide gauge data and GPS measurements, *Earth Planet. Sc. Lett.*, 439, 39-47, <https://doi.org/10.1016/j.epsl.2016.01.027>, 2016.

Santamaría-Gómez, A., Bouin, M.-N., Collilieux, X., and Wöppelmann, G.: Correlated errors in GPS position time series: Implications for velocity estimates, *J. Geophys. Res.-Sol. Ea.*, 116, B01405, <https://doi.org/10.1029/2010JB007701>, 2011.

Santamaría-Gómez, A., Gravelle, M., Collilieux, X., Guichard, M., Míguez, B. M., Tiphaneau, P., and Wöppelmann, G.: Mitigating the effects of vertical land motion in tide gauge records using a state-of-the-art GPS velocity field, *Global Planet. Change*, 98-99, 6-17, <https://doi.org/10.1016/j.gloplacha.2012.07.007>, 2012.



Scharroo, R., Leuliette, E., Lillibridge, J., Byrne, D., Naeije, M., and Mitchum, G.: RADS: Consistent multi-mission products, in: Proceedings of Symposium on 20 Years of Progress in Radar Altimetry, 24-29 September 2012, Venice, 20, 59-60, 2012.

Scharroo, R. and Smith, W. H. F.: A global positioning system-based climatology for the total electron content in the ionosphere, *J. Geophys. Res.-Space*, 115, <https://doi.org/10.1029/2009JA014719>, 2010.

SL_cci, The Climate Change Initiative Coastal Sea Level Team. Coastal sea level anomalies and associated trends from Jason satellite altimetry over 2002-2018. *Sci Data* 7, 357 (2020). <https://doi.org/10.1038/s41597-020-00694-w>

SL_cci_b, The Climate Change Coastal sea level team (2020): ESA Sea Level Climate Change Initiative (Sea_Level_cci): Altimeter along-track high resolution sea level anomalies in some coastal regions (2002-2018) from the JASON satellites, v1.1. Centre for Environmental Data Analysis, *date of citation*. doi:10.5270/esa-sl_cci-xtrack_ales_sla-200206_201805-v1.1-202005. http://dx.doi.org/10.5270/esa-sl_cci-xtrack_ales_sla-200206_201805-v1.1-202005

Woodworth, P. L., Hunter, J. R., Marcos, M., Caldwell, P., Menéndez, M., and Haigh, I.: Towards a global higher frequency sea level dataset, *Geosci. Data J.*, 3, 50-59, <https://doi.org/10.1002/gdj3.42>, 2016.

Wöppelmann, G. and Marcos, M.: Vertical land motion as a key to understanding sea level change and variability, *Rev. Geophys.*, 54, 64-92, <https://doi.org/10.1002/2015RG000502>, 2016.



End of the document